A RAPID NUMERICAL METHOD FOR 3D AERO DYNAMICS DESIGN OF COMPRESSOR BLADE ROW (APPLICATION TO A LOW SPEED EXPERIMENTAL MULTI-IDENTICAL-STAGE COMPRESSOR DESIGN)

Naixing Chen, Hongwu Zhang, Yanji Xu and Weiguang Huang
Institute of Engineering Thermophysics
Chinese Academy of Sciences, Beijing China
P.O. Box 2706, Beijing 100080, CHINA
E-mail: nxc@etpserver.etp.ac.cn , Fax: 08610-62575913)

Abstract

A numerical method for 3D aerodynamic design of a compressor blade row in the present paper is developed based on the iterative calculations by successively using a grid generation method and a N.S. solver. At beginning the flow rate, the pressure ratio and the geometry of meridian pattern were given. The span-height distributions of inlet and exit pitch-wise-averaged flow angles of the blade row were obtained by the preliminary calculations. They are served to be the target parameters of the present calculation. Successively using a grid generation method and a N.S. solver, a 3-D blade configuration can be obtained. The optimal design can be obtained by a set of calculations with different span-height distributions of inlet and exit pitch-wise-averaged flow angles of the blade row. As an example an experimental compressor with three identical stages is shown.

1 INTRODUCTION

Due to the progress of the computer sciences and computational techniques the use of computational methods for designing the blade configurations of turbomachinery has become more attractive in the turbomachinery community. The blade geometry can be estimated by fluid mechanics theory, such as conformal mapping, singularity methods, and various methods based on using stream function, potential function or their combinations, and Euler or N.S. solutions [1,2,3] .

The present work is based on the iterative calculations by successively using a grid generation method and a N.S. solver. The target distributions of inlet and outlet flow angles along span height are obtained from the calculation at the preliminary design stage or are given. Then, a 3D grid system can be obtained only by giving (1) geometry of meridian pattern; (2) inlet and outlet blade angle distributions along span-height; (3) thickness distributions along blade height. From numerical calculation by N.S. solver all aerodynamics parameters can be obtained. If the flow angle distributions calculated along the span height do not agree with the target ones, the blade angle distributions are revised and the grid system is generated again. The iterative procedure is carried on by successively using these two codes until the calculated and the target ones are closed each to other. From a set of calculations of different pitch-wisely averaged span-height distributions of inlet and outlet flow angles an optimal blade configuration can be obtained.

An experimental axial compressor with three identical stages is shown as an example. The detailed data of the flow field, including pressure, temperature and flow angles, and the performance data, including global total pressure, global total temperature ratios and global adiabatic efficiency

via flow rate, can be also obtained. Here only limited data of the final results are demonstrated in the paper due to the limitation of the paper length.

2 DESCRIPTION OF THE METHOD

The basic idea of the present rapid design method for a compressor blade row, which principle scheme is shown in Fig.1, is successively to solve a grid generation method and 3D N.S. direct solution method with target inlet and outlet flow angle variations along span height. As shown in the figure, at the first design stage the total flow rate and the total pressure ratio are given for a given rotation speed and a given geometry of meridian pattern. The span-height distributions of pitch-wisely averaged inlet and outlet flow angles along span height are obtained by the preliminary calculations. They are taken to be the target parameters. The adiabatic efficiency is given which is required from the global performance. Then, using a grid generation method a 3D configuration of the blade row is obtained and a 3D-grid system can be also generated. It can be served as the meshes for the N.S. calculation. The next step is to calculate the flow field with the N.S. solver. Comparing the target parameters with these calculated pitch-wise-averaged results gives us newly revised data for the next grid generation calculation. Then, the N.S. method is used again after generating the new 3D-grid system by the same grid generation method. These calculations are repeated until the inlet and outlet flow angle distributions are satisfied to the requirement. If the adiabatic efficiency calculated is less than the given, changing the flow angle distributions, the above calculations are repeated again until the optimal results are obtained.

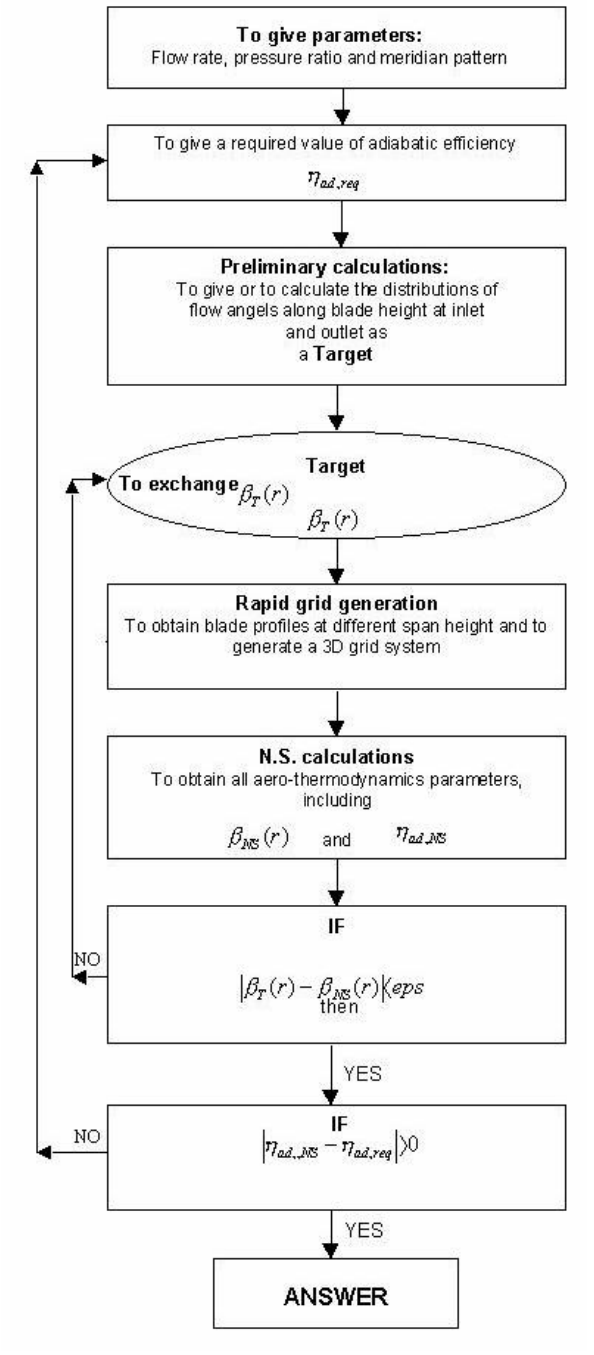

Fig.1 Principle scheme

2.1 Grid Generation Method

A special grid generation method (the code name is 'Lisa') was proposed by the authors and used for the blade design. Using present grid generation code enables us to generate a 3d-grid system by given blade angle distribution and geometry of meridian pattern. The grid system is generated very rapidly within few minutes on personal computer. It can be served as the meshes for 3D calculation by N.S. solver. In the present method the camber line and the thickness distribution at different blade height are expressed by two polynomials as:

$$r\varphi = a_0 + a_1 z_x + a_2 z_x^{2\,2} \qquad (1a)$$

or

$$\beta = a\tan(a_1 + 2a_2 z_x)^2 \qquad (1b)$$

and

$$\bar{y} = b_0 + b_1\bar{x} + b_2\bar{x}^2 + b_3\bar{x}^{3\,2} \qquad (2)$$

where: r is radii and φ is angular coordinate; β is blade angle; z_x is relative meridian length; $\bar{y}$ denotes the relative blade thickness; $\bar{x}$ denotes relative length of blade camber line; a_0, a_1, a_2, a_3, and b_0, b_1, b_2, b_3 are the coefficients of above equations. They are defined by the boundary conditions of equations (1a), (1b) and (2). By changing the coefficients, b_0, b_1, b_2, b_3, different thickness distribution can be obtained. Axial and radial distributions of blade thickness are given according to the structure stress requirement. In the present grid generation method, the radius of leading and trailing edges can be given arbitrarily by the designer.

2.2 N.S. Solution Method

The second step is to calculate the flow field by a N.S. solver. The N.S. solution method used is a three-dimensional pressure correction method coupled with a $\kappa - \varepsilon$ turbulence model. By the way, any kind of N.S. solver for low-speed turbomachinery flow field can be applied for this solution.

3 CALCULATION EXAMPLE

As an example, an experimental three-stage compressor is designed by the present method. In order to simplify the manufacturing process and to reduce the cost, the compressor had better be composed of three identical stages. So the design compressor is consisted of an inlet guide vane row, three rotor blade rows and three stator blade rows. The preliminary computations for all aerodynamic parameters, including flow angles along span height, are based on the simplified radial equilibrium method. Then, the 3D meshes of each blade row are generated by the grid generation method. The grid systems for the first three blade rows are demonstrated in Figs. 2-4.

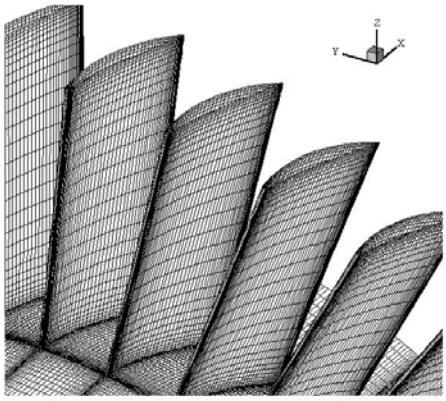

Fig.2 Inlet guide vanes

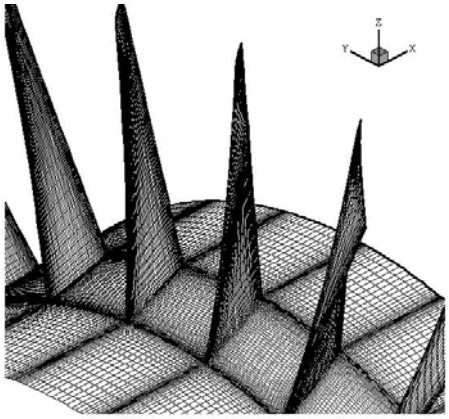

Fig.3 Rotor blades

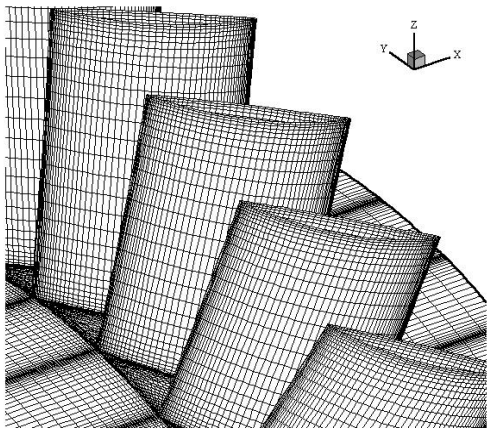

Fig.4 Stator blades

The flow field of the compressor is calculated as a whole by the N.S. solver. If the circumferentially averaged calculated flow angles do not satisfy the designed, the geometrical blade angles at inlet and outlet of blade row are required to be revised, and the grid generation is repeated again. The iteration procedure of

successive use of grid generation and N.S. solution is repeated again until the present solution is closed to the target. The principles of revising blade inlet and outlet angles are as follows:

(1) Inlet blade angle distribution along span height for the inlet guide vane (IGV) row are set to be zero and the inlet blade angle distributions for the other blade rows are taken to be equal to the exit flow angles from the preceding blade rows calculated by the N.S. solver. This means that the incident angles for the blade rows are set to be zero;

(2) Outlet blade angles for next iteration are taken as the sum of the present blade angle and the difference between designed and present blade angle with relaxation;

(3) There is no boundary layer separation occurred.

The present numerical study includes (1) inlet single stage compressor - three blade row calculation as a whole, which includes an inlet guide vane row, a rotor and a stator blade rows; (2) two-stage compressor - five blade row calculation including an inlet guide vane row and two identical stages; (3) three-stage compressor - seven blade row calculation including an inlet guide vane and three identical stages.

3.1 Inlet Single Stage – Three-Blade-Row Calculation

Because the objective of the design is to obtain a compressor with three identical stages, the pitch-wisely-averaged outlet flow angles along the blade height from inlet guide vane (IGV) row and stator blade row should be approximately equal each other. Fig.5 shows the final iteration results of outlet flow angles of IGV, rotor and stator blade rows. The negative flow angles represent the relative flow angle, and the positive values represent the absolute flow angles. The figure shows that the absolute flow angles of IGV and stator blade row are agreed well with each other along the major part of the blade height except near the hub region.

Fig.6 shows the velocity vector schemes and particle traces on the 10% blade height surface from the hub in the stator passage. As shown in the figure there is an obvious flow separation near the trailing edge of stator suction surface. This separation just occurs below 20% blade height. Because of this separation, the absolute flow angles on the stator outlet surface are different from those on the IGV outlet surface as shown in fig.5. In the later calculations we will observer that the flow separation disappears if we add a blade row behind the last stator blade row.

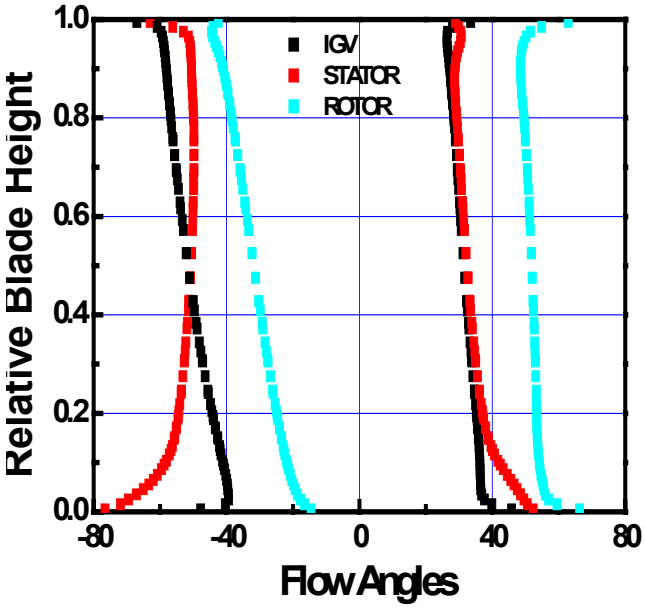

Fig.5 Flow angle distributions along blade height

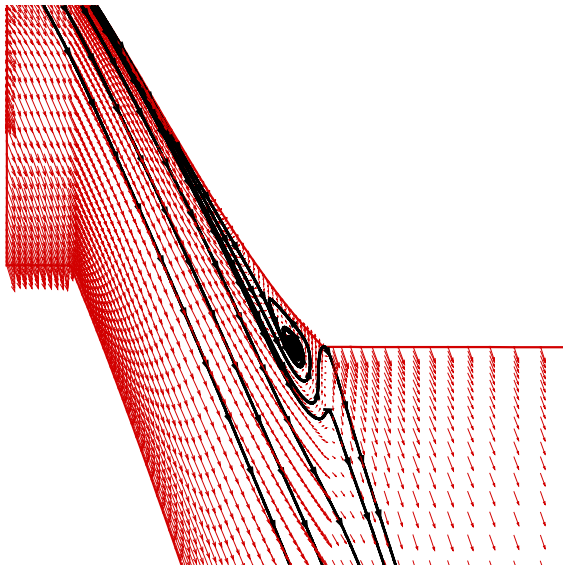

Fig.6 Velocity vectors schemes and particle traces

The static pressure distributions on pressure and suction surfaces of the blades at near-hub-, mid-

and near-tip span height for the IGV, rotor and stator blade rows calculated are shown in Fig.7. As shown in the figure it is seen clearly that the blade load for rotor and stator blade rows is increased with increasing the span height.

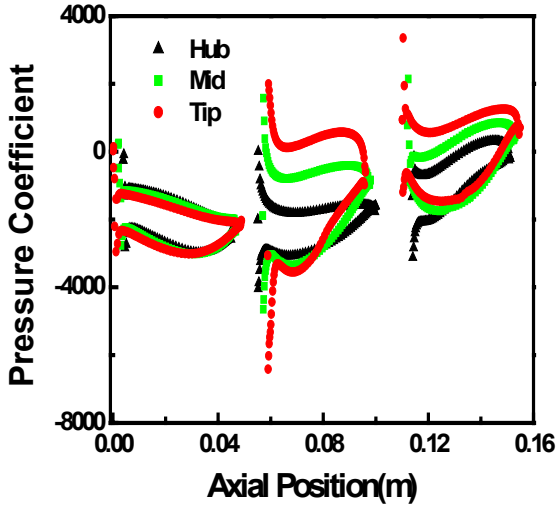

Fig.7 Static pressure distributions on blade surfaces

3.2 Two-Stage Compressor – Five-Blade-Row Calculation

In the present calculation the flow field within five blade rows (an IGV and two identical stages) is calculated as a whole, i.e., the computational domain includes inlet and outlet regions, an IGV row and two rotor and two stator blade rows. There is no separation in the stator passage of the first stage in this case. It means that the flow pattern in the first stage, especially of the stator blade row, is changed and different from the single stage calculation when the second stage was added behind the first stage.

Fig.8 shows the final iteration results of the pitch-wisely averaged outlet flow angles of IGV row, rotor blade and stator blade rows of first and second stages. As in fig. 5, the negative flow angles represent the relative flow angle, and the positive values represent the absolute flow angles. The figure shows that the absolute flow angles of IGV and first stator are agreed well with each other along almost the whole blade height, although some difference also exist under 10% blade height. Compared with fig. 5, the largest difference decreased from 10 degree to about 3 degree near the hub. On the other hand, the relative flow angles of IGV and first stator also have big differences, but the maximum difference value also decreased from 40 degree to less than 30 degree compared to the single stage calculation. Unfortunately, although the differences of the outlet flow angles between the IGV and first stator decreased, the differences of the absolute outlet flow angles between second stator and IGV grow dramatically under 30% blade height. The maximum different value is about 40 degree that occurs near the hub.

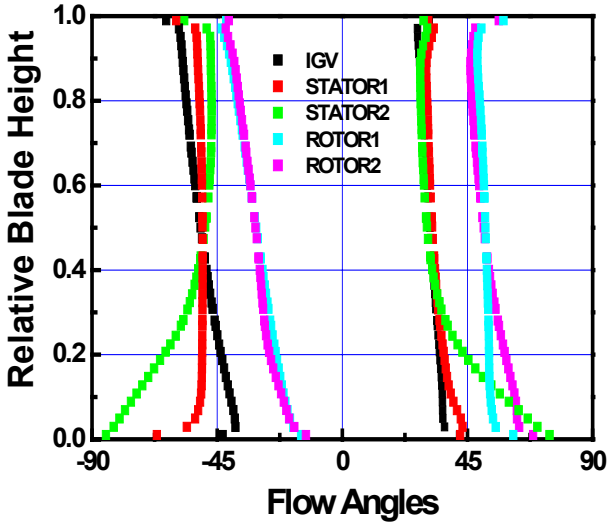

Fig.8 Flow angles along blade height

Fig.9 and fig.10 show the velocity vectors and particle traces on the 10% blade height surface from the hub in the first and second stator passages, respectively. Compared to fig. 6, the flow separation in the first stator passage occurred in the single stage calculation disappeared. Because of the disappearance of the flow separation, the outlet flow angles of first stator are more close to the IGV as shown in fig.8. Fig.10 shows an obvious flow separation near the trailing edge of second stator suction surface. Because of this separation, the flow angles on the stator outlet surface are different from those on the IGV outlet surface as shown in fig.8.

The static pressure distributions on pressure and suction surfaces at near-hub-, mid- and near-tip-span height for the IGV, first rotor, first stator, second rotor and second stator calculated are shown in Fig.11.

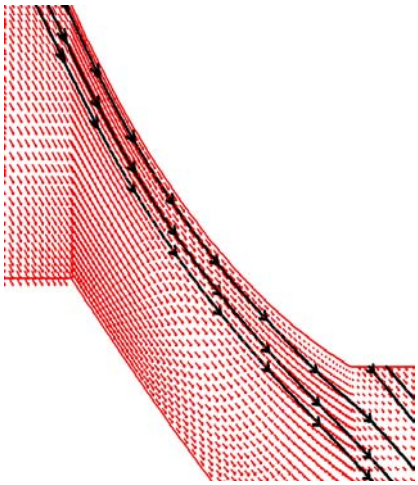

Fig.9 Velocity vector schemes and particle traces in 1st stator

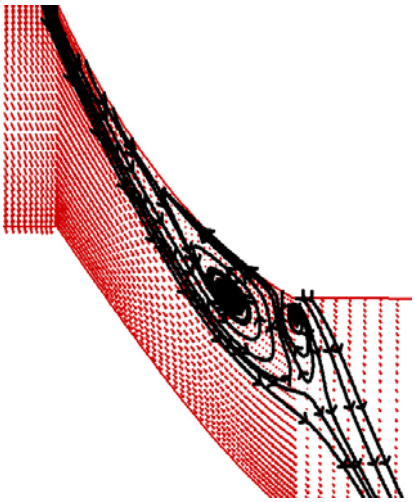

Fig.10 Velocity vector schemes and particle traces in 2nd stator

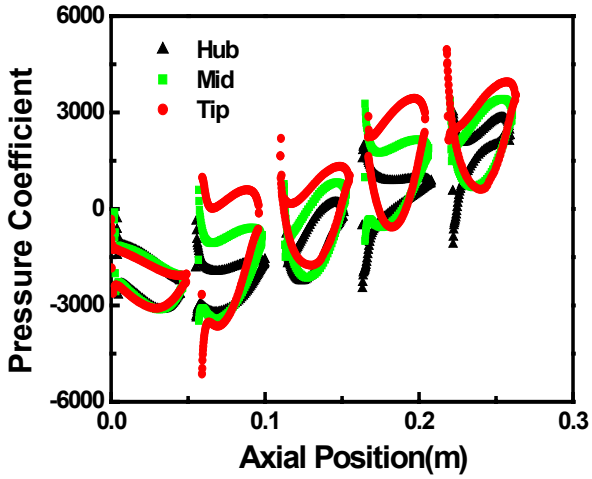

Fig.11 Static pressure distributions on blade surfaces

3.3. Three-Identical-Stage Compressor Calculation

The final objective of this example is to design a three-stage test axial flow compressor facility. So the whole compressor calculation including total seven blade rows was performed.

Fig.12 shows the final iteration results of outlet flow angles of IGV, first stage, second stage and third stage. Compared to fig.5 and fig.8, fig.12 shows that the absolute flow angles of IGV, first stator and second stator are agreed well with each other along almost the whole blade height as in fig.5. Moreover, the values of first and second stator are almost identical. Although there exists differences between the IGV and the third stator below 30% blade height, the maximum differential value on the blade root decreased from 40 to about 20 degree compared to fig.8. On the relative flow angles side, as shown in figs.5 and 8, large differences also exist between IGV and the downstream stators. The maximum difference occurs between the IGV and the last stator blade row. It means the differences on the relative flow angles between IGV and stators increase along the flow direction. The relative outlet flow angles of the three rotors are almost identical along the whole blade height.

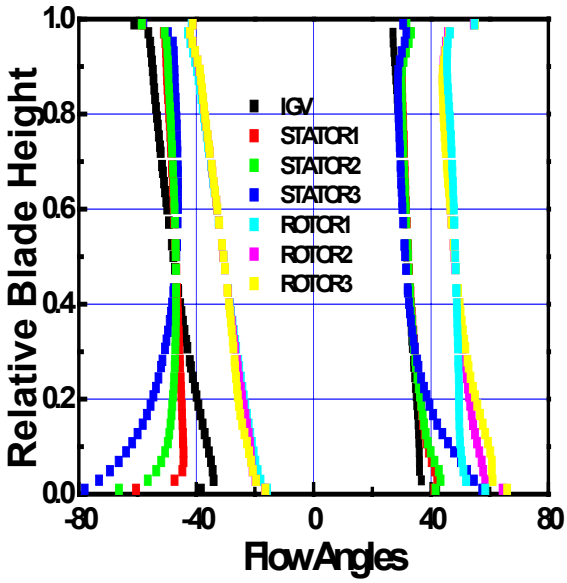

Fig.12 Flow angles along blade height

Fig.13, fig.14 and fig.15 show the velocity vectors and streamlines on the 10% blade height surface from the hub in the first, second and third stator passages, respectively. Fig.13 shows no

flow separation occurred in the first stator passage. Fig.14 shows no flow separation in the second stator. Compared with fig.10, this separation is obviously strong. Fig.15 shows an obvious flow separation near the trailing edge of the third stator suction surface. Because of this separation, the flow angles on the stator outlet surface are different from those on the IGV outlet surface as shown in fig.12.

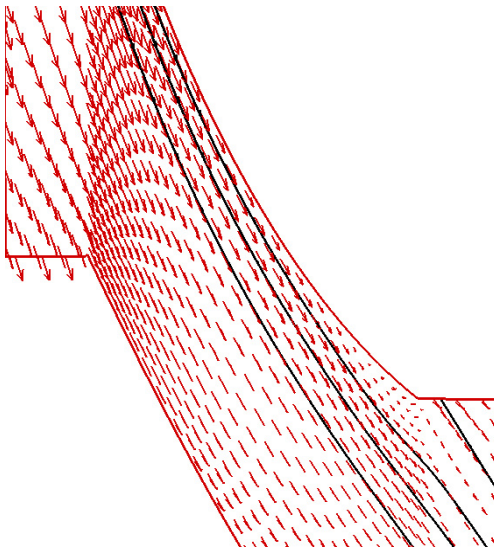

Fig.13 Velocity vector schemes and particle traces in 1st stator

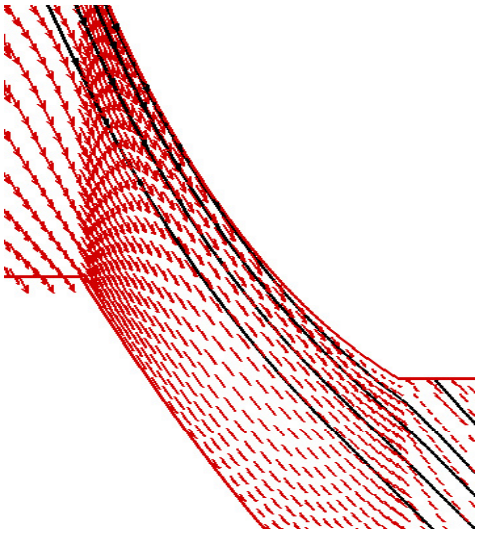

Fig14 Velocity vector schemes and particle traces in 2nd stator

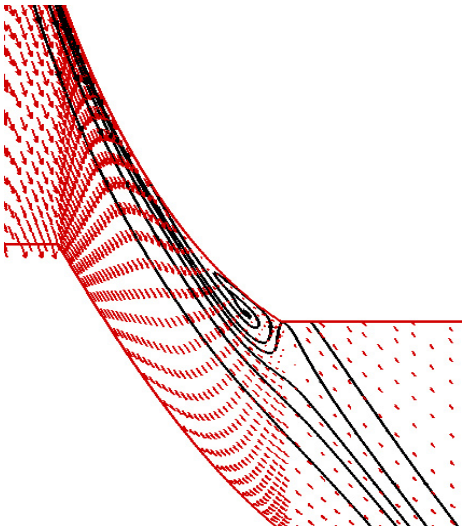

Fig.15 Velocity vector schemes and particle traces in 3rd stator

It can be derived from the previous calculations that the existence of the downstream blade row can avoid the separation occurrence in the stator passage of the same stage. So if an outlet guide vane is added behind the last stator, it could be believed that the separation in the third stator also can be diminished or completely avoided.

Fig.16, fig.17 and fig.18 show the static pressure contours on three different S1 surfaces of revolution: near-hub, mid-span and near-tip, respectively. The static pressure distributions on pressure and suction surfaces of near-hub-, mid- and near-tip- span height for the whole compressor calculation are shown in Fig.19.

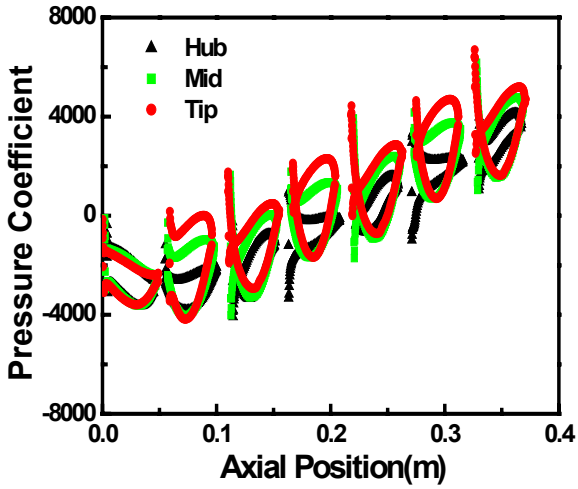

Fig.19 Static pressure distributions on blade surfaces

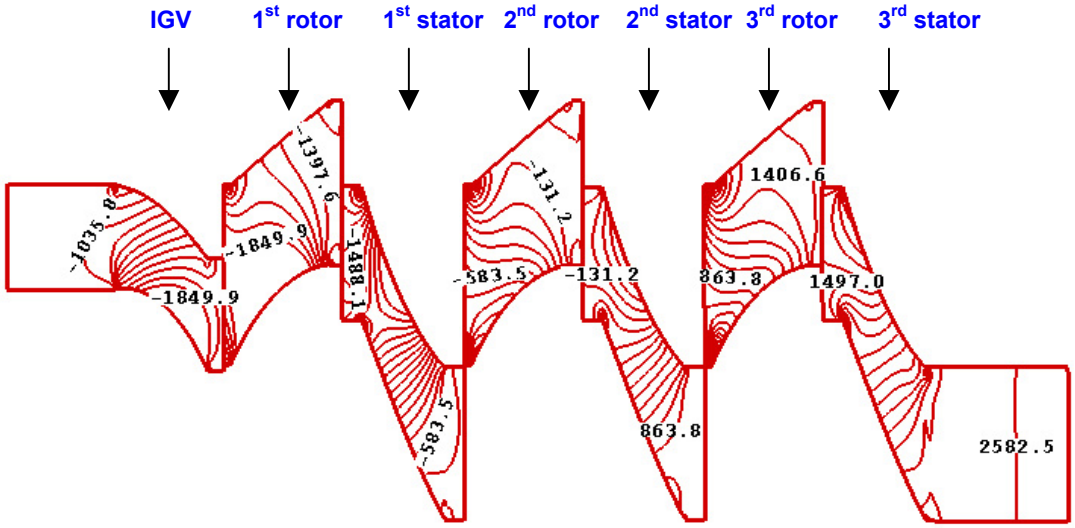

Fig.16 Static pressure contours on the near-hub surface of revolution

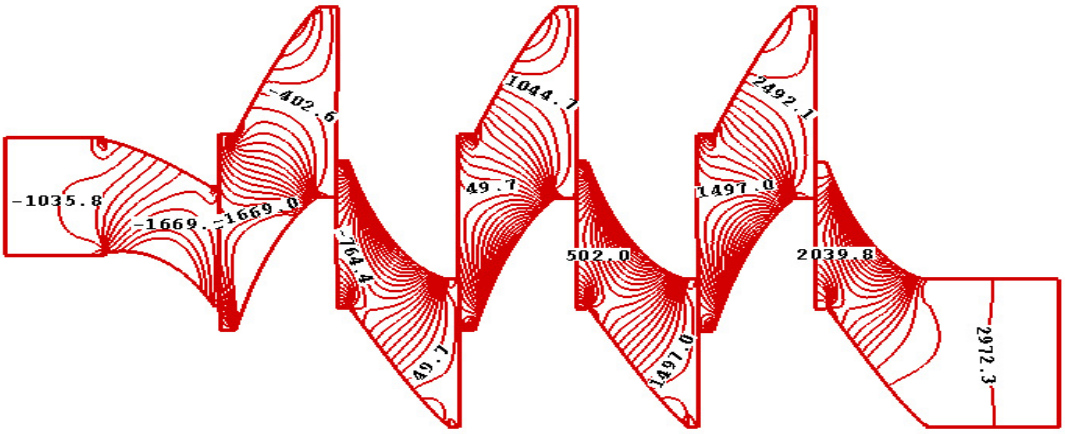

Fig.17 Static pressure contours on the mid-surface of revolution

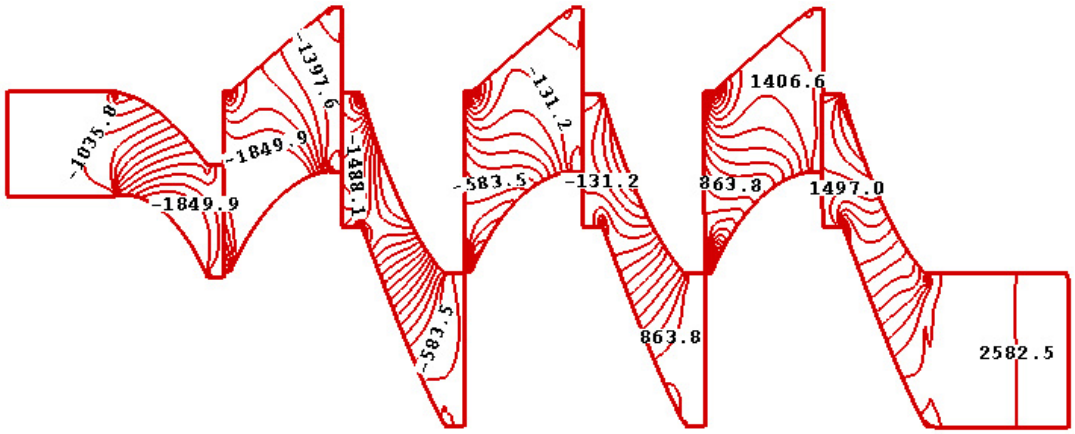

Fig.18 Static pressure contours on the near-tip surface of revolution

3.4. Global performance

Fig.20 shows the performance of the three-identical-stage compressor. According to this figure, the design condition was fixed as mass flow rate: 6.85kg/s, total pressure ratio: 1.0406, and efficiency: 83.3%. If the adiabatic efficiency does not satisfy the required, changing the span-height distributions of flow angles of the blade rows the similar calculation procedure is repeated again until the optimal results can be obtained.

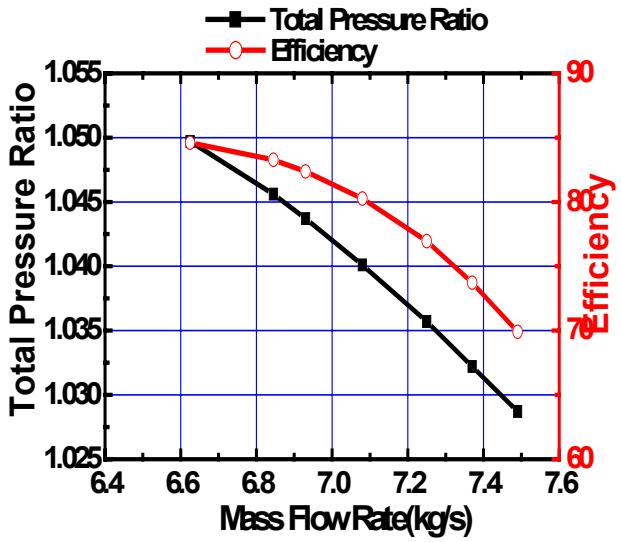

Fig.20 Performance of experimental compressor

4. CONCLUSIONS

The present method was successfully applied to design a three-stage test compressor facility. The calculation results proved that the method is robust enough. By the present idea, the grid system is generated very rapidly within few minutes on personal computer. It can be served as the meshes for 3D calculation by N.S. solver. Any N.S. solvers can be combined with this grid generation system. Then, the N.S. solver calculations results in that all aerodynamic parameters in detail can be obtained. The method can be served to evaluate the quality of the designed machine.

5 ACKNOWLEDGEMENT

The research in this paper is funded by the project of NKBRSF (No. G1999022306). This support is gratefully acknowledged.

REFERENCES

[1] Chen, Naixing. From *Recent Development of Aerodynamic Design Methodologies – Inverse Design and Optimization*, pp.113-145, Edited by K. Fujii and G.S. Dulikravich, Friedr. Vieweg & Sohn Verlagsgesellschaft mbH, Braunschweig /Wiesbaden, 1999.

[2] Chen, N.X., Chen, John J.J.J. and Chen, X.D. *Proceeding, the 7th International Rotational Machinery Conference*, pp.1386-1393, 1998.

[3] Chen, N.X., Xu, Y.J., Huang, W.G., Ma, H.W. and Jiang, H.K. *Proceeding of the Fourth International Symposium on Experimental and Computational Aerothermodynamics of Internal Flow*, Contributed Paper, No.009, , Aug. 31-Sept. 2, 1999.